

# Turbulence Characteristics and Interaction between Particles and Fluid in Particle-Laden Open Channel Flows

Iehisa Nezu, M.ASCE,<sup>1</sup> and Ryoukei Azuma<sup>2</sup>

**Abstract:** Mechanism of sediment transport is composed of complicated interactions between turbulent flow, particle motion, and bed configurations. Of particular significance is the interaction between turbulence and particle motion, although turbulence measurements of particle-laden two phase flow have been a problem for a long time, especially in the near-wall region. In this study, simultaneous measurements of both the particles and fluid (water) were conducted in particle-laden two phase open channel flows by means of a discriminator particle-tracking velocimetry. The mean velocity and turbulence characteristics for fluid and particles each were examined in comparison with those in clear-water (particle-free) flow, together with previous existing data measured by laser Doppler anemometer and phase Doppler anemometer. The relative velocity and the turbulence modulation, which are the most important topics in two phase-flow approach, were revealed by varying the particle diameter and specific density. The fluid-sweeps are more contributory to the motion of particles than the fluid ejections in the near-wall region. In turn, the particle-sweeps transport the high momentum to the carrier fluid and enhance the turbulence intensities of fluid.

**DOI:** 10.1061/(ASCE)0733-9429(2004)130:10(988)

**CE Database subject headings:** Turbulence; Open channel flow; Particle interactions; Two phase flow.

## Introduction and Review

Particle-laden flows are encountered in a wide range of flow configurations and thus have been paid great attention in fluid mechanical and hydraulic community. In rivers, the mechanism of sediment transport is composed of complicated interactions between turbulent flow, sand-particle motion, and bed configurations. Of particular significance is the interaction between turbulent flow and sand-particle motion. Turbulence plays an essential role in suspended sediment transport, and in turn sand-particle motion influences the velocity profiles and the resistance law, which are very important for practical purposes, e.g., Lyn (1991) and Nino and Garcia (1996). A lot of earlier studies on suspended sediment-laden flow are based on one-fluid model as a passive contaminant scalar, and the change of the von Karman constant versus the sediment concentration has been discussed on the basis of velocity profiles of mixture fluid measured by conventional intrusive probes such as Pitot tubes, e.g., see Guo and Julien (2001). One of the most important achievements in such an one-fluid model is an expression of suspended sediment concentration, i.e., the Rouse formula, which was derived from diffusion theory, e.g., see Yalin (1972), and the Rouse formula is very useful even now in hydraulic engineering.

<sup>1</sup>Professor, Dept. of Civil and Global Environmental Engineering, Kyoto Univ., Kyoto 606-8501, Japan. E-mail: nezu@nezu.gee.kyoto-u.ac.jp

<sup>2</sup>PhD Student, Dept. of Civil and Global Environmental Engineering, Kyoto Univ., Kyoto 606-8501, Japan. E-mail: azuma@nezu.gee.kyoto-u.ac.jp

Note. Discussion open until March 1, 2005. Separate discussions must be submitted for individual papers. To extend the closing date by one month, a written request must be filed with the ASCE Managing Editor. The manuscript for this paper was submitted for review and possible publication on February 28, 2003; approved on April 12, 2004. This paper is part of the *Journal of Hydraulic Engineering*, Vol. 130, No. 10, October 1, 2004. ©ASCE, ISSN 0733-9429/2004/10-988-1001/\$18.00.

It has been suggested strongly that the velocity distribution and turbulence characteristics in particle-laden flows may be different from those of particle-free flows due to fluid-particle interactions. However, simultaneous measurements of solid particles and fluid have been essentially difficult to be conducted by conventional intrusive probes. Therefore, some investigations on fluid-particle interactions have been conducted by numerical simulations. Squires and Eaton (1990) conducted simulations of two phase solid-liquid flow in homogenous and isotropic turbulence using a direct numerical simulation (DNS), and pointed out that the particles caused the turbulent energy in the higher wave numbers of spectrum to increase relative to the lower ones, and consequently the turbulence modulation might be induced by the fluid-particle interactions, which is called the “two-way coupling” between particles and carrier fluid. Elghobashi (1994) and Crowe et al. (1996) have reviewed the numerical simulation models for particle-laden two phase flows and discussed the importance of two-way coupling models.

With the advent of laser Doppler anemometer (LDA) and phase Doppler anemometer (PDA), accurate noninstructive measurements have been possible in particle-laden flows. Rogers and Eaton (1990, 1991) have first conducted turbulence measurements in boundary layer of vertical air flows by using 4 mW He-Ne LDA, in which glass and copper beads were used as particles. They found the turbulence modulation similar to that predicted by Squires and Eaton (1990). Kulick et al. (1994) conducted similar measurements in vertical air duct flows using the same particles as used by Rogers and Eaton (1991). The other type flow configurations in particle-laden two phase flows have highlighted the turbulence modulation in pipes and jets for pneumatic transport, in which almost carrier fluid is gas. Gore and Crowe (1989) reviewed previous existing experimental data of jets and pipes, and found that turbulence intensity of fluid might be enhanced by particles when the particle diameter  $d_p$  is larger than  $0.1 l_e$ , whereas it might be suppressed by particles when  $d_p/l_e < 0.1$ , in

which  $l_e$  is the integral length scale of turbulence. However, Elghobashi and Truesdell (1993) queried the criterion of Gore and Crowe (1989) and suggested from DNS of isotropic grid turbulence that the turbulence intensity would be increased for  $d_p/l_e \geq 0.001$ .

In contrast, particle-laden open channel flow is one of the most complicated but most challenging flow configurations to us since it plays an essential role in sediment transport. This is because the particle concentration becomes much larger closer to the bed due to gravity and thus the fluid–particle interactions will be more enhanced there. Furthermore, coherent structures such as ejections and sweeps will influence such fluid–particle interactions most significantly. Sumer and Deigaard (1981), Rashidi et al. (1990), and Nino and Garcia (1996) suggested by flow visualization that the ejections and sweeps in the near-wall region governed the fluid–particle interactions, and stressed the essential importance of two phase-flow approach in suspended-sediment transport on the basis of modern turbulence theory including bursting phenomena in open channel flow.

According to modern turbulence theory, open channel flow is composed of two regions; the inner-wall region ( $y/h \leq 0.2$ ) and the outer region ( $y/h \geq 0.2$ ), in which  $y$  is the vertical coordinate and  $h$  is the flow depth, e.g., see Nezu and Nakagawa (1993). The inner-wall region is further composed of the viscous sublayer, the buffer layer and the log-law layer, and controlled by the inner-wall variables such as the friction velocity  $U_*$  and the kinematic viscosity  $\nu$ ; that is “the law of the wall.” In contrast, the outer region is controlled by the outer variables of the flow depth  $h$  and the maximum mainstream velocity  $U_{\max}$ . The velocity in the other region deviates upward from the log-law, and is described empirically by the log-wake law, in which the wake-strength parameter  $\Pi$  is a key measure as a deviation from the log-law. The bursting phenomena occur most violently in the inner-wall region and generate the turbulent energy most significantly. Its energy is diffused into the outer region and dissipated near the free surface. The mutual interaction between the inner wall and outer regions is very important for fully understanding of open channel turbulence although the former is active essence of turbulence and the latter is more passive one.

Particle-free open channel flow, which we call here the “clear-water flow” has to be cited as an inevitable reference and compared with particle-laden open channel flow, as pointed out by Lyn (1991), Muste (2002), and others. One example of clear-water-flow measurements is offered by Nezu and Rodi (1986) who measured open channel turbulence with 2 W Ar-ion LDA, and they found that the von Karman constant  $\kappa$  is the universal value of  $\kappa=0.412$ , while the value of  $\Pi$  depends on the Reynolds number. Since  $\Pi$  is the outer parameter, it also depends on the aspect ratio of the channel that correlates with secondary currents, as well as on the pressure gradients and the other outer variables.

It has been much more difficult to conduct turbulence measurements in particle-laden open channel flows even with nonintrusive LDA than those in boundary layers and pipes mentioned previously. This is because the experimental flume was relatively large scale and the sediment concentration was very high near the bed if sand particles were used, and consequently we may not be able to measure the inner-wall region with LDA because of blocking laser beams by dense particles. Nevertheless, Lyn (1991, 1992) conducted turbulence measurements in sediment-laden open channel flows with He–Ne LDA, in which sand particles were used over the rough bed. He found that the carrier fluid velocity was shifted downward from the clear-water log-law when the sediment concentration  $C$  increased, and suggested that

the von Karman constant  $\kappa$  might decrease with  $C$ , the result of which had been pointed out in earlier studies by Pitot tubes. However, the measurement region of Lyn was the outer region rather than the inner-wall region. Cioffi and Gallerano (1991) measured particle-laden open channel flow with a PDA, which enables us to measure both particle velocity and concentration simultaneously if the particle is sphere. They used glass beads and found that the value of  $\kappa$  was the same as used in clear-water flow, i.e., no change of the von Karman constant was observed even in particle-laden flow. However, they also could not measure the inner-wall region in detail as compared with the outer-region measurements. The utility of PDA in hydraulic experiments has greatly advanced fundamental research on sediment transport although the particles have to be spherical. Best et al. (1997) successfully conducted simultaneous measurements of both fluid velocity and particle velocity with 100 mW Ar-ion PDA in particle-laden open channel flow over the rough bed covered by  $d_p=0.22$  mm glass beads. They used the same glass beads as suspended-sediment particles and found that the value of  $\kappa$  decreased slightly as compared with clear-water flow although only two runs of experiments of low concentrations were conducted;  $\kappa=0.39$  was obtained. Of particular significance in Best et al. (1997) is that turbulence intensity might be enhanced near the bed and its property might correlate with Stokes number of particles, which will be discussed later. Further, Bennett et al. (1998) measured fluid–particle velocities over upper stage plane beds by using the same PDA, in which the sediment concentration was much higher than that of Best et al. (1997). Unfortunately, both of them could not measure the near-wall region where the bursting phenomena occur most violently. This is probably because: (1) the laser power was relatively low (100 mW) and (2) the bed wall was covered by roughness elements, i.e., no smooth-wall condition. Muste and Patel (1997) developed a 15 mW LDA system incorporated with a unit for particle-size discrimination. Natural sands were used as sediment particles and the channel bottom was rough. They found that the average velocity of sand particles was smaller than that of fluid (water) in the measurement region of  $y/h > 0.15$  (almost outer region). This fact suggests that there exists a relative velocity difference between particles and fluid and thus the fluid–particle interactions may affect flow structures. These suggestions are also obtained by Best et al. (1997) and Bennett et al. (1998).

As mentioned before, the fluid–particle interactions and the bursting phenomena both occur most violently in the inner-wall region of  $y/h < 0.2$ , but unfortunately it is much more difficult to measure this inner-wall region than the outer region. One of the techniques to overcome these difficulties is the use of lighter particles than glass particles, such that particles are more apt to be lifted up to the outer region at even low mainstream velocities or low Reynolds numbers. Kaftori et al. (1995, 1998) conducted simultaneous measurements of fluid and particle velocities in particle-laden open channel flow using Ar-ion LDA incorporated with amplitude discriminator. Of particular significance was the use of polystyrene beads of  $\rho_p=1.05$ . The diameter  $d_p$  was possible to change in a wide range of 0.1, 0.275, and 0.9 mm, because it is very important to examine the particle response time against the time scale of turbulence, as will be discussed later. Kaftori et al. (1995) pointed out a surprising result that the average velocity of particles was larger than that of carrier fluid very near the wall, indicating a change of fluid–particle interactions and a possibility of complicated interaction between bursting phenomena and particle motion, as suggested by Nino and Garcia (1996).

**Table 1.** Comparison of Particles in Particle-Laden Open Channel Flows

Researchers	$d_p$ (mm)	$\rho_p$ (g/cm <sup>3</sup> )
Present data	0.3, 0.5, 0.8, 1.0, 1.3	1.05 polystyrene and 1.15 (PMMA/PS)
Lyn (1991, 1992)	0.15, 0.19, 0.24	2.65 (natural sands)
Kaftori et al. (1995, 1998)	0.1, 0.28, 0.9	1.05 (polystyrene)
Best et al. (1997)	0.22	2.6 (glass beads)
Muste and Patel (1997)	0.21–0.25	2.65 (natural sands)
Bennett et al. (1998)	0.22	2.6 (glass beads)

In addition to nonintrusive point measurements such as LDA and PDA, recent flow-visualization techniques such as particle-image velocimetry (PIV) and particle-tracking velocimetry (PTV) may be applied to measure the particle motion in flows. The most notable advantage of PTV over LDA is the possibility of measurements of larger particles, by which the fluid-particle interactions and the particle-response property will be able to be examined. In this study, turbulence measurements of polystyrene particles and fluid (water) were conducted with PTV in particle-laden open channel flows over the smooth bed, which was covered by no roughness elements. The particle and fluid data were separated by discriminating the occupied area sizes of particle images and water tracers on a charge coupled device (CCD) camera. The diameter of particles  $d_p$  was changed in a wide range of  $d_p=0.3\text{--}1.3$  mm. The specific density  $\rho_p$  was chosen as  $\rho_p=1.05$  and 1.15. The hydrodynamic characteristics of both the inner wall and outer regions were investigated intensively and compared with the existing data available from the other researchers (see Table 1).

## Experimental Setup and Hydraulic Conditions

### Experimental Equipment

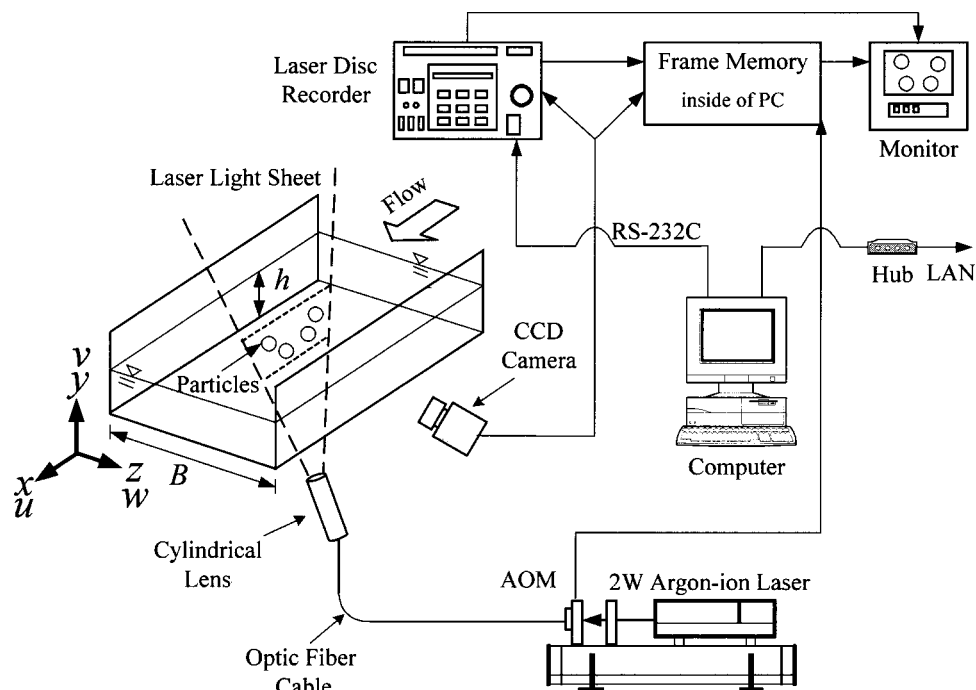
The experiments were conducted in a 10 m long, 15 cm wide, and 30 cm deep tilting flume, as shown in Fig. 1.  $x$ ,  $y$ , and  $z$  are the

streamwise, vertical, and spanwise coordinates, respectively. The instantaneous velocity components of  $\vec{u}(t) \equiv U+u(t)$  and  $\vec{v}(t) \equiv V+v(t)$  were measured by PTV, where the capital and small letters denote the time-averaged component and the turbulent fluctuating one, respectively.

A 2 W Ar-ion laser beam was guided through an optical fiber cable and illuminated the flow vertically from the channel bottom as a 2 mm thickness laser light sheet (LLS) (see Fig. 1). The LLS can be adjusted by the computer-controlled acousto-optic modulator, in which the emission interval and its duration were adjusted in the range  $\Delta t=3\text{--}6$  ms and 0.5–0.9 ms, respectively, as schematized in Fig. 2. Pairs of images of particles were taken by a highly sensitive CCD camera (SONY), installed near the side-wall, with a time interval of 1/30 s and resolution of  $512 \times 480$  pixels. The images were recorded by a digital laser-disk recorder (SONY). The present PTV system was the same as the PIV system used by Nezu and Onitsuka (2001) except for the software.

### Experimental Conditions

The hydraulic conditions are summarized in Table 2; here,  $d_p$  is the particle diameter and  $\rho_p$  is its density,  $h$  the water depth,  $U_m$  the mean bulk velocity,  $R \equiv U_m h / \nu$  the Reynolds number, and

**Fig. 1.** Experimental setup and particle-tracking velocimetry arrangements

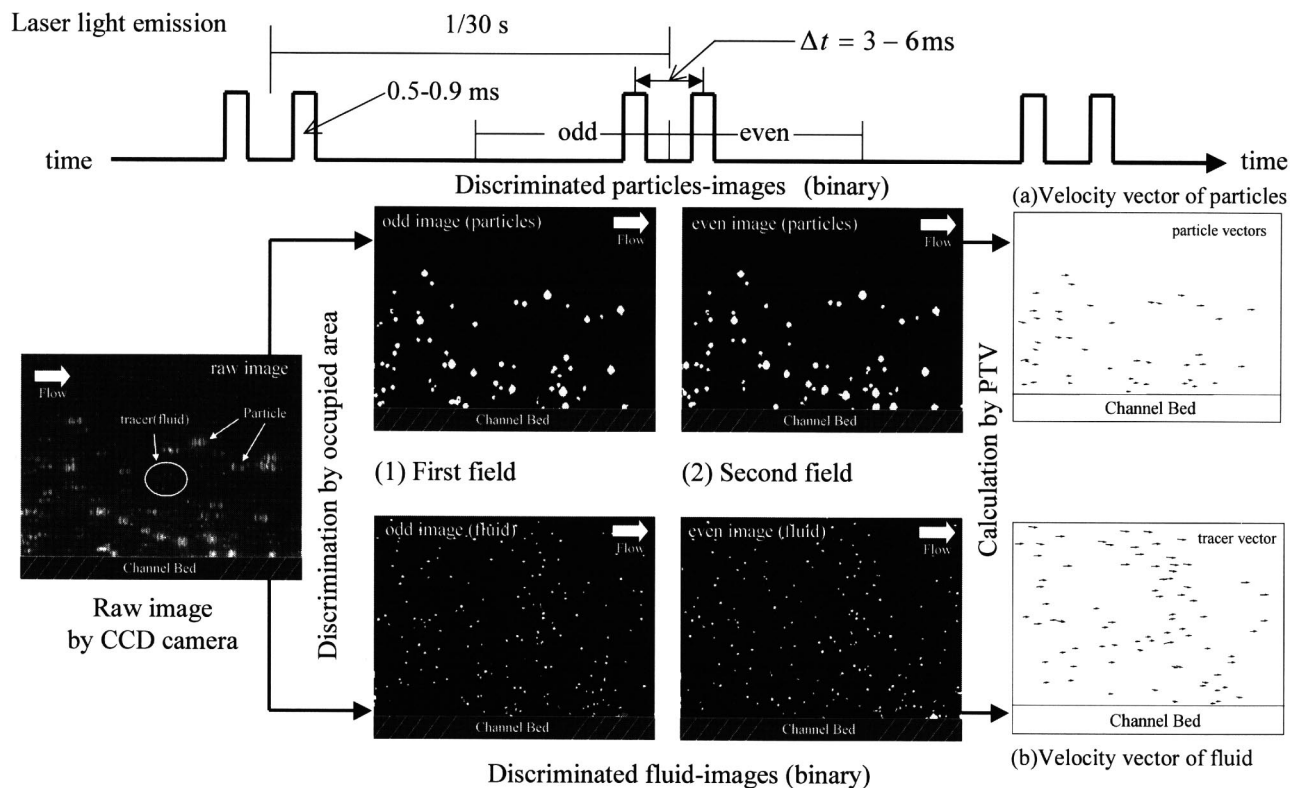


Fig. 2. Image processing of particles and fluid

$F \equiv U_m / \sqrt{gh}$  the Froude number.  $U_*$  is the friction velocity, which is the most important velocity scale and its evaluation method will be discussed later.

Two series of experiments, (A) and (B) were conducted (Table 2). For Group A, the range of the measurement region was the whole flow depth (whole-depth series), whereas for Group B the near-wall region from the channel bed up to 20 mm (near-wall series, the closeup pictures) was measured. The actual length of 1 pixel corresponded to 0.153 mm for Group A and 0.0303 mm for Group B, respectively. In the experiments of A, the diameter  $d_p$  of polystyrene particles ( $\rho_p=1.05$ ) was changed in a wide range, i.e.,  $d_p=0.3, 0.5, 0.8, 1.0,$  and  $1.3$  mm, and the depth-

averaged volumetric concentration  $\bar{C}$  of these particles was set at 0.03–0.32%, in which no deposition was observed on the smooth bed. The flow depth  $h=5.0$  cm and the bulk mean velocity  $U_m=28$  cm/s were set the same among all cases of A. Therefore, the turbulence length scale  $l$  of the fluid was almost the same in all experiments of A, and in contrast the particle diameter  $d_p$  was changed in a wide range. The effect of particle size on fluid-particle interactions will be revealed because  $d_p/l$  is a significant factor in mechanism of turbulence modulation, as pointed out by Gore and Growe (1989) and Elghobashi and Truesdell (1993).

In Group B, both kinds of particles, i.e., polystyrene ( $\rho_p=1.05$ ) and polymethyl methacrylate/polystyrene (PMMA/PS)

Table 2. Hydraulic Conditions and Evaluated Values

Case	$d_p$ (mm)	$\rho_p$ (g/cm <sup>3</sup> )	$h$ (cm)	$U_m$ (cm/s)	R ( $\times 10^4$ )	F	$U_*$ (cm/s)	$\kappa$	$R_*$	$d_p^+$	$\bar{C}$ (%)
(A) Whole-depth series											
CW1	—	—	5.0	28.1	1.4	0.4	1.49	0.412	756	—	—
PS03	0.3	1.05	5.0	28.0	1.4	0.4	1.48	0.400	751	4.5	0.03
PS05	0.5	1.05	5.0	28.1	1.4	0.4	1.47	0.399	746	7.4	0.08
PS08	0.8	1.05	5.0	28.1	1.4	0.4	1.52	0.397	771	12.3	0.11
PS10	1.0	1.05	5.0	27.9	1.4	0.4	1.49	0.396	755	15.1	0.13
PS13	1.3	1.05	5.0	27.9	1.4	0.4	1.48	0.394	750	19.5	0.32
(B) Near-wall series											
CW2	—	—	5.0	24.6	1.23	0.35	1.32	0.411	670	—	—
PS05w	0.5	1.05	5.0	24.6	1.23	0.35	1.33	0.409	675	6.7	—
PS08w	0.8	1.05	5.0	24.6	1.23	0.35	1.32	0.407	670	10.7	—
CW3	—	—	5.0	50.0	2.50	0.71	2.63	0.410	1334	—	—
PM05w	0.5	1.15	5.0	50.0	2.50	0.71	2.65	0.404	1344	13.4	—
PM08w	0.8	1.15	5.0	50.0	2.50	0.71	2.63	0.401	1334	21.3	—

( $\rho_p=1.15$ ) were used to examine the influence of specific density although it was difficult to change the value of  $\rho_p$  widely. The fluid-particle interactions and the correlations with bursting phenomena were investigated in detail as a parameter of the wall unit, i.e.,  $\nu/U_*$ , in which the superscript + is used here, e.g.,  $y^+ \equiv yU_*/\nu$ . The case name of PS and PM denotes the polystyrene and PMMA/PS, respectively. Clear water flows (CW1, CW2, and CW3) are particle-free, which are compared with particle-laden flows for references.

The diameter and specific density of tracer particles (Nylon 12) for carrier fluid were 0.1 mm and 1.02, respectively. These tracer particles were scattered uniformly in the water of the recirculating flume. The test section was located 7 m downstream of the channel entrance. The measuring time of PTV was 60 s and the time interval between two laser pulses in the picture was  $\Delta t = 4$  ms, similar to methods used by Nezu and Onitsuka (2001).

## Calculation Methods of Particle and Fluid Velocity

### Discrimination between Particle and Fluid Data

A discrimination technique between particle and fluid on a snapshot image of a CCD camera first has to be developed for simultaneous measurements. Two methods of discrimination are considered: (1) the particle-color discrimination (discriminated by coloring particles) and (2) the particle-size discrimination, where particles are discriminated by their occupied area. The particle-size discrimination was adopted in this study and is explained here.

Fig. 2 shows an example of the raw image and processing images of solid particles and fluid tracer for case PS13. The present recording system is the National Television Standards Committee for images. The raw image consists of the odd and even scanning lines. First of all, the brightness of the raw image was adjusted most suitably, and separated into the odd and even fields with the time interval  $\Delta t$ . The separated images were binarized, and each particle and fluid tracer in the field was then discriminated by using a threshold value of the occupied area of particles.

For this particle-size discrimination, it is important to set a resolution of the CCD camera reasonably. In this study, the length of 1 pixel in the CCD camera corresponded to 0.153 mm for Group A and 0.0303 mm for the closeup Group B. The occupied area of the smallest sediment particle of  $d_p=0.3$  mm was larger than 4 pixels for Group A, while that of fluid tracer was 1 pixel. Therefore, it was easy to discriminate automatically the solid particles and fluid, as indicated in Fig. 2. Even if only part of particle was captured as the fluid tracer in the odd field and its most part was captured as a solid particle in the even field, such data were omitted from analysis, and vice versa in the even-odd fields. So, we can expect that the crosstalk of discrimination between particle and fluid would be negligibly small even in the case of the smallest particle, because of the very short time interval  $\Delta t = 4$  ms between the odd and even fields, as shown in Fig. 2. This particle-size discrimination was applied reasonably to all cases of the present experiments.

### Particle-Tracking Velocimetry Algorithm

Nezu et al. (1999) conducted PTV measurements of sand particles over a gravel bed in open channel flow by making use of the four-fields-image algorithm, in which the target particle was

tracked in the four consecutive images by using a Kalman filter, which is one of the most popular methods in PTV. It was, however, difficult to track sand-particle motion near the bed by the four-fields-image algorithm, because these motions were quite complicated so that sand particles moving toward the bed sometimes rebounded from the bed. Further, the time interval of the four fields, i.e., 4/30 s, was comparatively large.

In contrast, Okamoto et al. (1995) developed a two-fields-image algorithm, based on the pattern matching of the particle cluster between two consecutive images using invisible elastic springs, a technique which they termed the "spring model." They pointed out that the spring model was useful even to flow fields including particles that both appeared and disappeared between the two consecutive images. Nezu et al. (2001) applied the spring model to a sediment-laden open channel flow, and concluded that this PTV model was reliable even in such a sediment-laden open channel flow. Therefore, the spring model was also adopted as PTV algorithm in the present study.

## Results and Discussion

### Clear-Water Flow

Fig. 3 shows the mean velocity profiles of clear-water flows for CW2 and CW3: the closeup PTV cases of the near-wall region (Table 2). These clear-water flows were measured with 2 W Ar-ion LDA (Dantec) as well as the present PTV for accurate comparison, although the LDA could measure the flow in the whole-flow depth, while the closeup PTV could measure it from the wall up to  $y/h=0.4$ . The symbols (LDA) and (PTV) in Fig. 3 indicate the results by LDA and PTV, respectively. The PTV data are shifted 5 units upwards in the vertical axis to avoid confusion. Three theoretical curves are included in Fig. 3

$$U_f^+ = y^+ \quad \text{for } y^+ \leq 5 \quad (1)$$

$$\frac{dU_f^+}{dy^+} = \frac{2(1 - y^+/R_*)}{1 + \sqrt{1 + 4\ell^{+2}(1 - y^+/R_*)}} \quad \text{for } 5 \leq y^+ \leq 30 \quad (2)$$

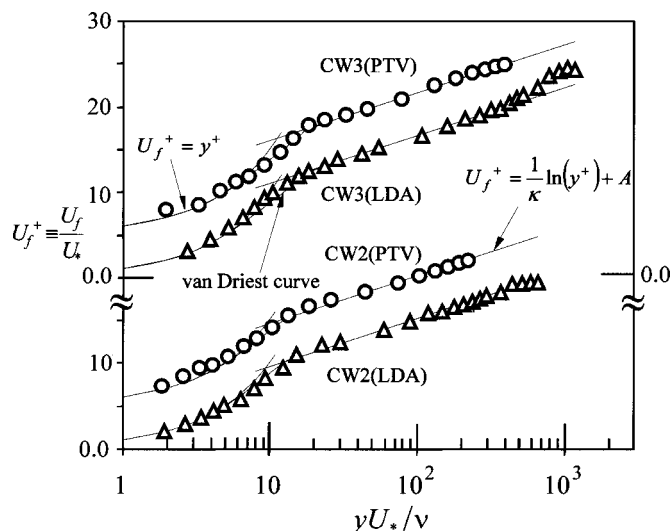


Fig. 3. Velocity profiles of clear-water flow (CW2 and CW3)

$$U_f^+ = \frac{1}{\kappa} \ln y^+ + A \quad \text{for } 30 \leq y^+ \leq 0.2R_* \quad (3)$$

in which  $U_f^+ \equiv U_f/U_*$  and  $y^+ \equiv yU_*/\nu$  = inner parameters normalized by the friction velocity  $U_*$  and the kinematic viscosity  $\nu$ ; and  $R_* \equiv hU_*/\nu$  = Reynolds number based on  $U_*$ . The subscripts  $f$  and  $p$  denote fluid and particles, respectively. Eq. (1) is the theoretical formula in the viscous sublayer of  $y^+ \leq 5$ , whereas Eq. (3) is the log-law that is satisfied in the inner-wall region of  $y^+ \geq 30$ , in which  $\kappa$  is the von Karman constant and  $A$  is the integration constant. No analytical solution is available in the buffer layer of  $5 \leq y^+ \leq 30$ , but a numerical curve (termed here the “van Driest curve”) is obtained from Eq. (2) by using the following van Driest damping function:

$$\ell^+ = \kappa y^+ \Gamma \quad \text{and} \quad \Gamma = 1 - \exp(-y^+/26) \quad (4)$$

in which  $\ell^+$  = mixing length.

According to Nezu and Rodi (1986), the value of  $U_*$  was evaluated from the measured Reynolds stress of fluid,  $-u_f v_f$ , in the following way. Fig. 4 shows the distributions of Reynolds stress for all cases in the present study. The clear-water flows were measured with both LDA and PTV. The theoretical curve in two-dimensional (2D) open channel flow, e.g., see Nezu and Nakagawa (1993) is given by

$$\frac{-u_f v_f}{U_*^2} = \left(1 - \frac{y}{h}\right) - \frac{dU_f^+}{dy^+} \quad (5)$$

If the viscous term is neglected, Eq. (5) is reduced to

$$\frac{-u_f v_f}{U_*^2} = 1 - \frac{y}{h} \quad (6)$$

Both LDA and PTV data are in good agreement with the theoretical curve of Eq. (5). Therefore, the friction velocity  $U_*$  was determined by an extrapolation of the measured Reynolds stress of  $-u_f v_f$  to  $y=0$ , i.e., using Eq. (6). These values of  $U_*$  evaluated from  $-u_f v_f$  are indicated in Table 2. The velocity profiles of  $U_f^+ \equiv U_f/U_*$  versus  $y^+ \equiv yU_*/\nu$  in Fig. 3 are normalized by these values of  $U_*$ . It should be noted that both LDA and PTV data in

Fig. 3 coincide well with the theoretical curve of Eq. (1). Further, von Karman constant  $\kappa$  can be determined from the log-law of Eq. (3) and these values are also indicated in Table 2. The present values of  $\kappa$  for clear-water flows agree quite well with the value of  $\kappa=0.412$  obtained by Nezu and Rodi (1986).

Figs. 3 and 4 demonstrate that the accuracy of the present PTV is sufficiently high for both the mean velocity and also second-order turbulence, such as Reynolds shear stress. Therefore, it is expected that this PTV can be applied to particle-laden open channel flows even in the near-wall region as well as in the outer region.

### Particle Concentration and Two Phase-Flow Approach

Elghobashi (1994) has classified gas–solid two phase flows on the basis of Stokes number  $St \equiv t_p/t_e$  and the volumetric particle concentration  $C$ , in which  $t_p$  is the particle response time and  $t_e$  is the turnover time of large eddy. Rogers and Eaton (1990) defined the particle response time  $t_p$  from the particle transport equation as follows:

$$t_p = \frac{\rho_p}{\rho_p - \rho_f} \frac{w_s}{g} \quad (7)$$

in which  $w_s$  = settling velocity of particle. For Stokes flow, it is theoretically given by

$$w_s = \frac{(\rho_p - \rho_f)g}{18\mu} d_p^2 \quad (8)$$

$$\therefore t_p = \frac{\rho_p d_p^2}{18\rho_f \nu} \quad \text{for Stokes flow} \quad (9)$$

Eq. (9) is often used in multiphase flow modeling because of the theoretical formula, e.g., see Elghobashi (1994) and Crowe et al. (1996). On the other hand, the eddy turnover time  $t_e$  is defined as  $t_e \equiv l_e/u'$ , in which  $u'$  is the turbulence intensity and  $l_e$  is the length scale of the energy containing eddies. The mixing length  $\ell$  estimated from Eq. (4) was approximately used here as  $l_e$  although it may be ambiguous in definition of eddy. In contrast,

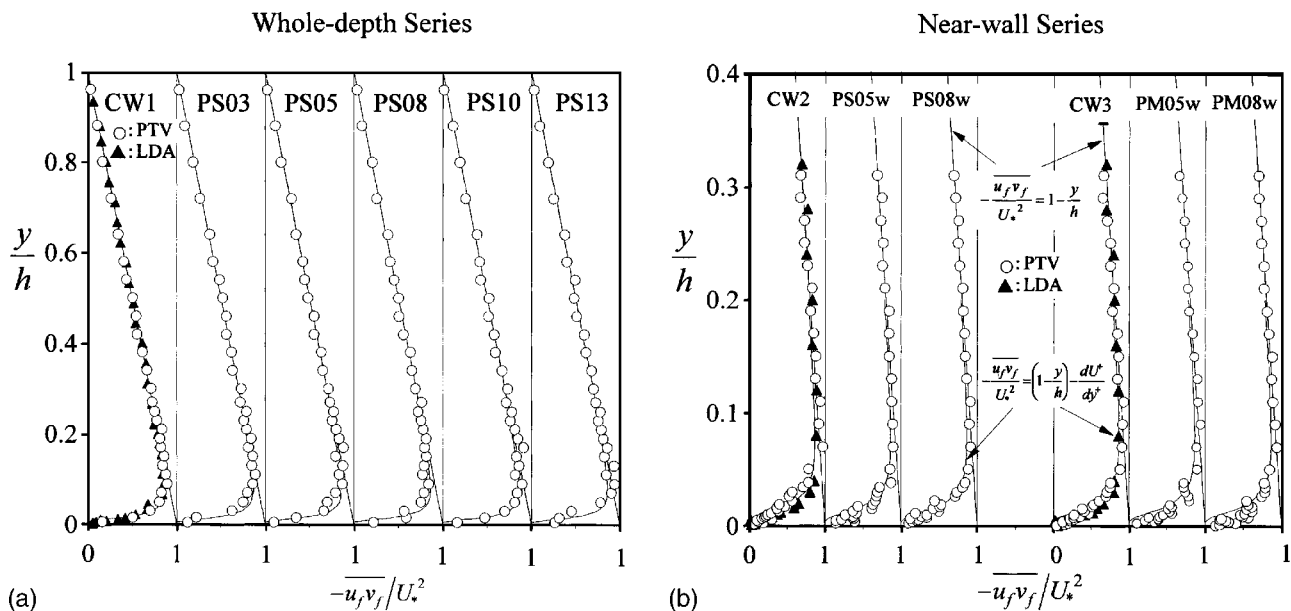


Fig. 4. Reynolds stress distributions in two phase open-channel flows

Best et al. (1997) used the Taylor microscale  $\lambda$  as  $l_e$ , although  $\lambda$  is not the macroscale of eddies.

The particle concentration  $C$  was evaluated by counting the number of particles in PTV images, which is similar to Best et al. (1997) although they used the PDA. Fig. 5 shows the vertical distributions of the volumetric particle concentration  $C$  for Group A. For references the Rouse formula is included in Fig. 5 and it is given by

$$\frac{C}{C_a} = \left[ \left( \frac{h_p - y}{h_p - a} \right) \left( \frac{a}{y} \right) \right]^Z \quad (10)$$

$$Z \equiv \frac{w_s}{\beta \kappa U_*}$$

in which  $h_p$ =thickness of suspended layer and  $C_a$ =particle concentration at  $y=0.05h_p$ , e.g., see Yalin (1972).  $\beta \equiv \varepsilon_s / \varepsilon_m$ =ratio of sediment diffusivity  $\varepsilon_s$  to momentum diffusivity (eddy viscosity)  $\varepsilon_m$ . The value of  $h_p$  was obtained from the PTV images, and these values are included in Fig. 5. In only case PS03 were the particles observed up to the free surface, i.e.,  $h_p=h$ , but in the other cases the particles were not suspended up to the free surface, i.e.,  $h_p < h$ . The value of  $\beta$  was determined so that the observed values of  $C$  might be most fitted to Eq. (10), and these values are also indicated in Fig. 5. The friction velocity  $U_*$  and von Karman constant  $\kappa$  that were used in Eq. (10) will be discussed later. The value of  $w_s$  was obtained from the settling-velocity experiments in still water. The observed values of  $C$  are in good agreement with the Rouse formula of Eq. (10) in the whole suspended layer, especially in the inner-wall region of  $y/h \leq 0.2$ . However, the value of  $\beta$  had to be selected as fairly larger than the expected value of  $\beta \approx 1.1$ . This suggests strongly that the particle-laden flow with larger grains than  $d_p=0.5$  mm cannot in principle be applied to Rouse's diffusion theory and has to be treated as two phase-flow approach, in which the relative velocity between particles and fluid is essentially important.

A diagram of  $St$  versus  $C$  for all cases of the present experiments, based on Elghobashi (1994), is shown in Fig. 6, where Eq. (9) was adopted here. He proposed the following classification of gas-solid flows:

One-way coupling for  $C < 10^{-6}$

Two-way coupling for  $10^{-6} < C < 10^{-3}$  (11)

Four-way coupling for  $C > 10^{-3}$

In one-way coupling, the particles have negligible effect on turbulence of fluid although fluid carries the particles. In two-way coupling, the momentum transfer from the particles is large enough to alter the turbulence structure, and thus the fluid-particle interaction plays an essential role in gas-solid transport. In the third regime, flows are referred to as dense suspensions, and in addition to the fluid-particle interaction, particle-particle collision takes place; he termed this the four-way coupling. This Elghobashi's classification of Eq. (11) may not be directly applied to aqueous sediment transport because the concentration is too small in gas-solid flows.

Of particular significance is that turbulence intensity is enhanced by particles, e.g., by vortex shedding behind them when  $St > 1$ , whereas it may be suppressed due to the increased dissipation by the presence of particles when  $St < 1$ . The criterion of  $St=1$  does not seem to be so strict because of ambiguous definition of eddy and the use of Eq. (9) that is valid only for Stokes flow. In fact, the observed values of  $w_s$  were fairly smaller than Stokes law of Eq. (8). However, the diagram of Fig. 6 qualitatively explains the importance of fluid-particle interactions in the present study. From Eq. (9), we can obtain as a criterion of enhancement of turbulence intensity

$$St \equiv \frac{t_p}{t_e} = \frac{1}{18} \frac{\rho_p}{\rho_f} \frac{u' d_p U_*}{\nu} \left( \frac{d_p}{l_e} \right) \equiv \frac{d_p^+}{9} \left( \frac{d_p}{l_e} \right) \geq 1 \quad (12)$$

in which the value of  $d_p^+ \equiv d_p U_* / \nu$  is indicated in Table 2. In the present experiments, we obtain from Eq. (12)

$$d_p / l_e \geq 9 / d_p^+ = (0.5 - 2) \quad (\text{for aqueous flows}) \quad (13)$$

Eq. (13) is consistent with the criterion of Gore and Crowe (1989) who used  $d_p / l_e > 0.1$  in gas-solid flows. Therefore, we can speculate that turbulence intensity will be enhanced by fluid-particle interactions near the wall in the present experiments. Further-

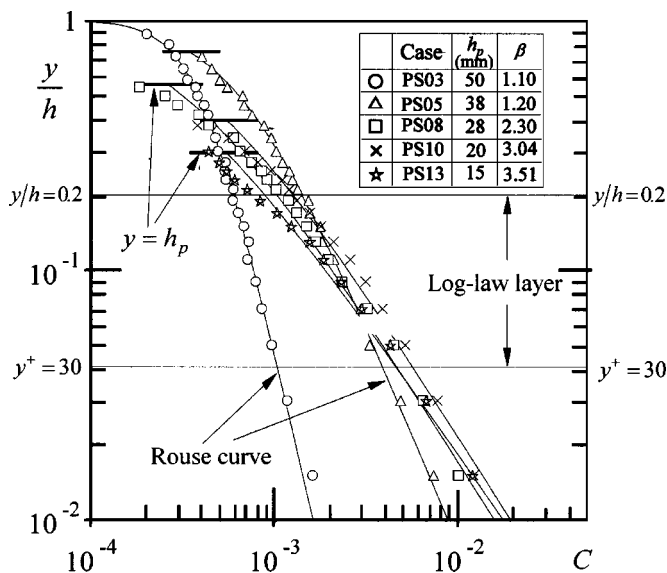


Fig. 5. Vertical distributions of volumetric particle concentration

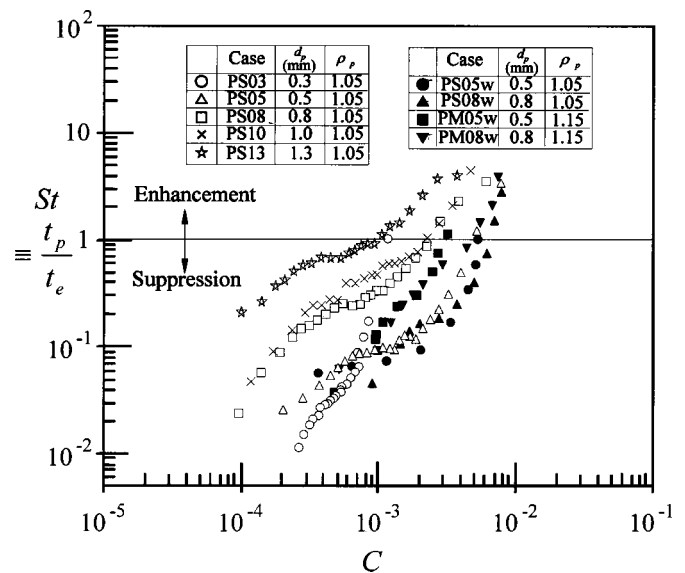


Fig. 6. Prediction of turbulence modulation

more, the effect of particle–particle collisions on turbulence intensity may not be negligibly small in the near-wall region where the concentration is much higher. These important suggestions from gas–solid flows are examined experimentally in the following sections.

### Evaluation of Friction Velocity

It is difficult to evaluate the friction velocity  $U_*$  from the log-law Eq. (3) in particle-laden open channel flows, because the von Karman constant  $\kappa$  for such flows is not perfectly established even now. Guo and Julien (2001) reviewed previous data of velocity profiles obtained by intrusive velocity measurements such as Pitot tubes, and suggested that the value of  $\kappa$  decreased with an increase of the sediment concentration, especially in dense suspended flows. In contrast, Muste (2002) reviewed the sources of bias errors in sediment-laden flow data and pointed out that the von Karman constant remains a universal value of  $\kappa=0.41$  even in dilute suspended flows on the basis of nonintrusive measurements such as LDA and PDA.

Fig. 4 shows the measured values of Reynolds stress of fluid,  $-u_f v_f$ , for all cases. The equation of motion in the outer region of 2D particle-laden open channel flow is reduced to

$$-\rho_f(1-C)\overline{u_f v_f} - \rho_p C \overline{u_p v_p} = \tau_w(1-y/h)$$

for  $y/h \geq 0.15$  (14)

$\tau_w$ =wall shear stress and the friction velocity  $U_*$  is defined as  $\tau_w \equiv \rho_f U_*^2$ . Since the concentration  $C$  is much smaller than 0.01 in the outer region (see Fig. 5), Eq. (14) is approximately reduced to

$$-\overline{u_f v_f} = U_*^2(1-y/h) \text{ for } y/h \geq 0.15 \quad (15)$$

Of course, Eq. (15) coincides with Eq. (6). We can recognize from Fig. 4 that the measured values of  $-u_f v_f$  are in good agreement with the theoretical linear curve of Eq. (15) in the outer region, and consequently the friction velocity  $U_*$  can be reasonably evaluated from Eq. (15) by the least squares method. These evaluated values of  $U_*$  for all cases are indicated in Table 2.

It is considered that this evaluation method of  $U_*$  is the most reliable if the Reynolds stress is measured. This method was also used by Lyn (1991), Kaftori et al. (1995), Muste and Patel (1997), Best et al. (1997), and Bennett et al. (1998). In contrast, Cioffi and Gallerano (1991) used the conventional formula,  $U_* = \sqrt{gRI}$ , in which  $R$  is the hydraulic radius and  $I$  is the channel slope. This conventional method is, however, apt to include experimental errors, as pointed out by Nezu and Rodi (1986), Muste and Patel (1997), and others.

### Mean Velocity Profiles of Fluid

Fig. 7 shows the mean velocity profiles of fluid  $U_f$  in particle-laden open channel flows, in which each case is shifted by 5 units upwards in the vertical direction. The clear-water data by Kaftori et al. (1995) and the particle-laden data in open channel flows by Best et al. (1997) and Bennett et al. (1998) (see Table 1) are included for comparison. The existence of the log-law is surely recognized in the inner-wall region of  $30 \leq y^+ \leq 0.2R_*$  for all cases, whereas the log-wake law is satisfied in the outer region. The data of Best et al. (1997) and Bennett et al. (1998) is shifted downward. A similar downward shift was observed by Muste and Patel (1997). This reason is not due to the presence of particles in suspension, but due to the effect of bed roughness. In contrast, the present data and Kaftori et al. (1995) data were obtained over the hydraulically smooth bed. Of particular significance is that the mean velocity  $U_f^+$  in the viscous region of  $y^+ \leq 10$  for particle-laden flow becomes larger and flatter than that for clear-water flow.

The von Karman constant  $\kappa$  was calculated from the log-law Eq. (3) and these values are also indicated in Table 2. It should be noticed that the value of  $\kappa$  decreases slightly with the depth-averaged concentration  $\bar{C}$ . A similar tendency was obtained by Best et al. (1997), Muste and Patel (1997), and Bennett et al. (1998) although the quantitative changes of  $\kappa$  are not yet established even now. Because the log-law is only valid in the log-law layer of  $30 \leq y^+ \leq 0.2R_*$  (see Fig. 5), it is better to adopt the concentration  $\bar{C}_{\log}$  averaged along only in the log-law layer, in-

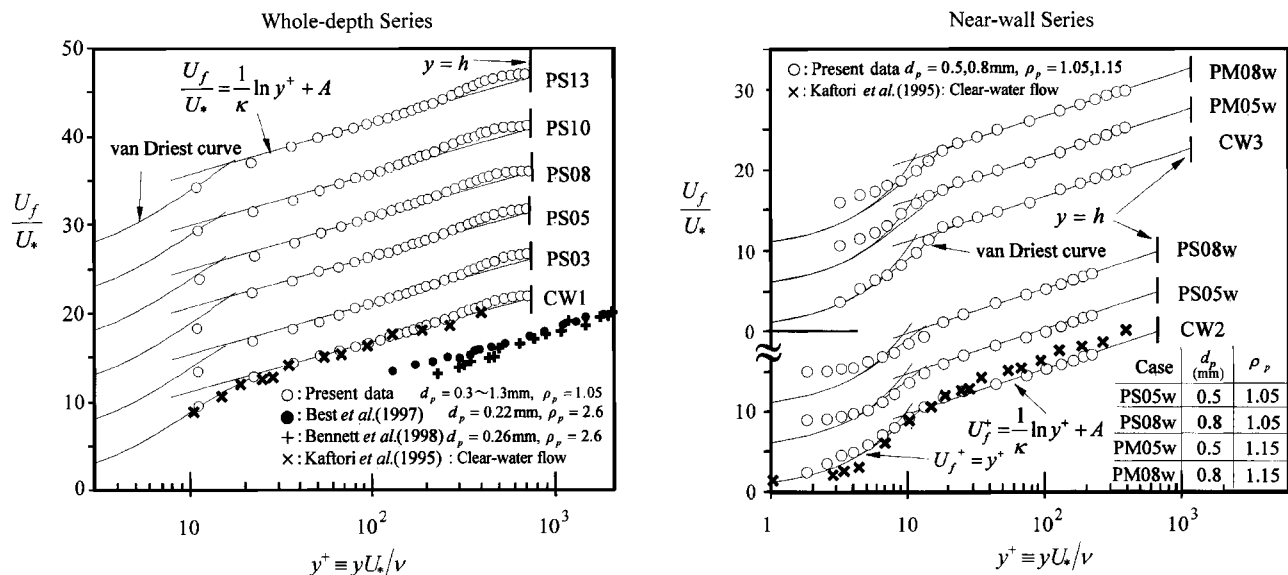


Fig. 7. Mean velocity profiles of fluid in two phase open-channel flows

stead of  $\bar{C}$ . Fig. 8 shows a tentative result of  $\kappa$  versus  $\bar{C}_{\log}$  for Group A. The von Karman constant  $\kappa$  decreases slightly with an increase of the concentration, and it is further necessary to reveal such variations quantitatively in wide ranges of concentration, specific density, and diameter of particles.

### Mean Velocity Profiles of Particles

Instantaneous velocity components ( $\tilde{u}_p, \tilde{v}_p$ ) of particles were measured by PTV, and the time-averaged velocity of particles  $U_p$  was obtained in the same manner as that of fluid  $U_f$ . However,  $U_p$  should not be identified as  $U_f$  due to the nonslip concept between particle and fluid boundaries, because the volume-averaged concept is used in such a two phase-flow approach, as pointed out by Elghobashi (1994) and Crowe et al. (1996). Fig. 9 shows the average velocity profiles of particles  $U_p$  for the near-wall series, together with previous data of Kaftori et al. (1995). The fluid-velocity formulae of Eqs. (1)–(3) are also included in Fig. 9 for comparison. The values of  $U_p$  were, of course, obtained only below the suspended-layer thickness, i.e.,  $y < h_p < h$ .

It is observed that the values of  $U_p$  are slightly smaller than the fluid log-law Eq. (3) and also coincident with Kaftori et al.'s (1995) data. In contrast, of particular significance is that the particle velocity  $U_p$  is larger than the fluid velocity  $U_f$  in the viscous region of  $y^+ \leq 15$ . That is to say, the relative velocity between particles and fluid is observed more significantly in the near-wall region, which will be discussed in the following section.

### Relative Velocity between Particles and Fluid

Fig. 10 shows the relative velocity,  $U_r \equiv U_f - U_p$ , for all cases, together with previous data of Kaftori et al. (1995), Best et al. (1997), Muste and Patel (1997), and Bennett et al. (1998). Fig. 10(a) uses the normal axis for the whole-depth series, while Fig. 10(b) uses the log axis for the near-wall series to highlight the near-wall region. It should be noticed from Fig. 10(a) that the average particle velocity  $U_p$  is slightly smaller than the fluid velocity  $U_f$  farther from the wall, irrespective of the specific density of particles  $\rho_p$ , i.e., polystyrene ( $\rho_p = 1.05$ ), glass ( $\rho_p = 2.6$ ), and sand ( $\rho_p = 2.65$ ). The present data are in good agreement with Kaftori et al.'s (1995) data, in which both of data are the same density of  $\rho_p = 1.05$ . Of particular significance is the effect of particle diameter  $d_p$  on the relative velocity  $U_r$ . The value of  $U_r$  increases with an increase of the particle diameter. This property is observed significantly in the inner-wall region of  $y^+ \leq 100$ , where the bursting phenomena occur violently, e.g., see Nezu and Nakagawa (1993). Evidently, this relative velocity induces the fluid-particle interactions and thus it is necessary to consider a two phase-flow approach in larger-particle-laden flows, say  $d_p \geq 0.5$  mm. Such a suggestion had also been inferred from Fig. 5, in which the cases of  $d_p \geq 0.5$  mm have  $\beta > 1.1$  that may contradict the hypothesis of Rouse's diffusion theory, as suggested by Bennett et al. (1998). In the two phase-flow approach, the particle response time  $t_p$  is a key factor to explain the fluid-particle interactions. When the particle Reynolds number  $R_p \equiv U_r d_p / \nu = (U_r / U_*) d_p^+ / \nu$  is smaller than the unity, the Stokes law is valid, i.e., Eq. (9). Because the value of  $R_p$  is, however, larger than the unity except for PS03 (see Table 2), Eq. (9) is invalid. Nevertheless, the following relation may be valid:

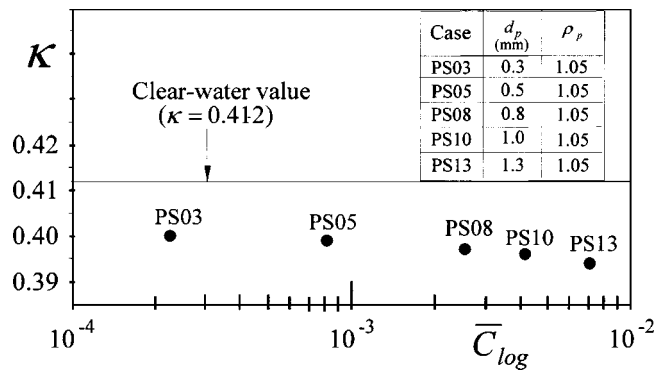


Fig. 8. von Karman constant versus particle concentration

$$t_p = K \frac{\rho_p d_p^2}{\rho_f \nu} \quad (16)$$

The coefficient  $K$  is smaller than  $1/18$  because of smaller settling velocity than the Stokes law Eq. (8). The particle response time  $t_p$  increases with the square of the diameter  $d_p$  and its increase is more significant than with the density  $\rho_p$ . The particles are able to follow the fluid motion when  $t_p \leq t_e \equiv l_e / u'$ , i.e.,  $St \leq 1$ , and otherwise the former cannot follow the latter. Since  $t_e^+ \equiv (l_e / u') (U_*^2 / \nu) = (l_e / h) R_* / (u' / U_*)$  is roughly equal to  $R_*$  in the outer region, the normalized value of  $t_p^+ \equiv t_p (U_*^2 / \nu) = K (\rho_p / \rho_f) d_p^{+2}$  becomes much smaller than  $t_e^+$  there. For example, in the largest case of PS13,  $t_p^+ = 399K$  becomes smaller than 22, whereas  $t_e^+$  is roughly equal to  $R_* = 750$  (see Table 2). Consequently, the particles can follow the fluid motion farther from the wall and the relative velocity  $U_r$  is reduced to be negligibly small. These characteristics have been numerically predicted by Pedinotti et al. (1992) who conducted a direct numerical simulation (DNS) of particle-laden horizontal channel flows although the one-way coupling was treated.

On the other hand, we now highlight the near-wall region in Fig. 10(b), which is much more complicated than the outer re-

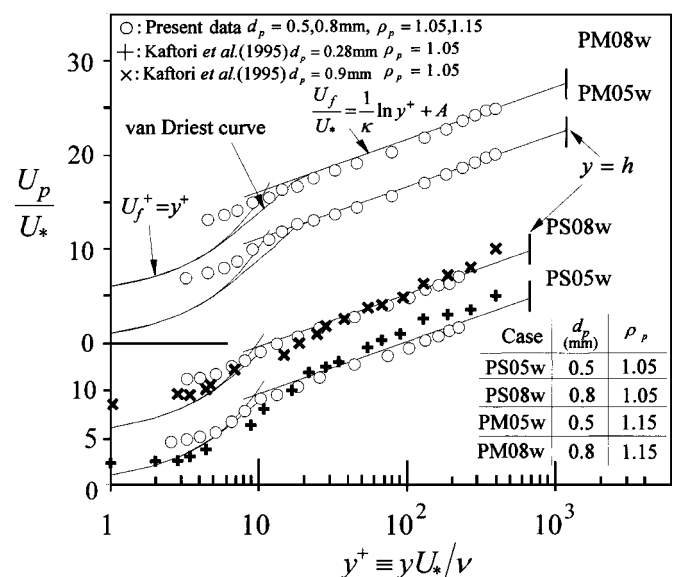


Fig. 9. Mean velocity profiles of particles in two phase open-channel flows

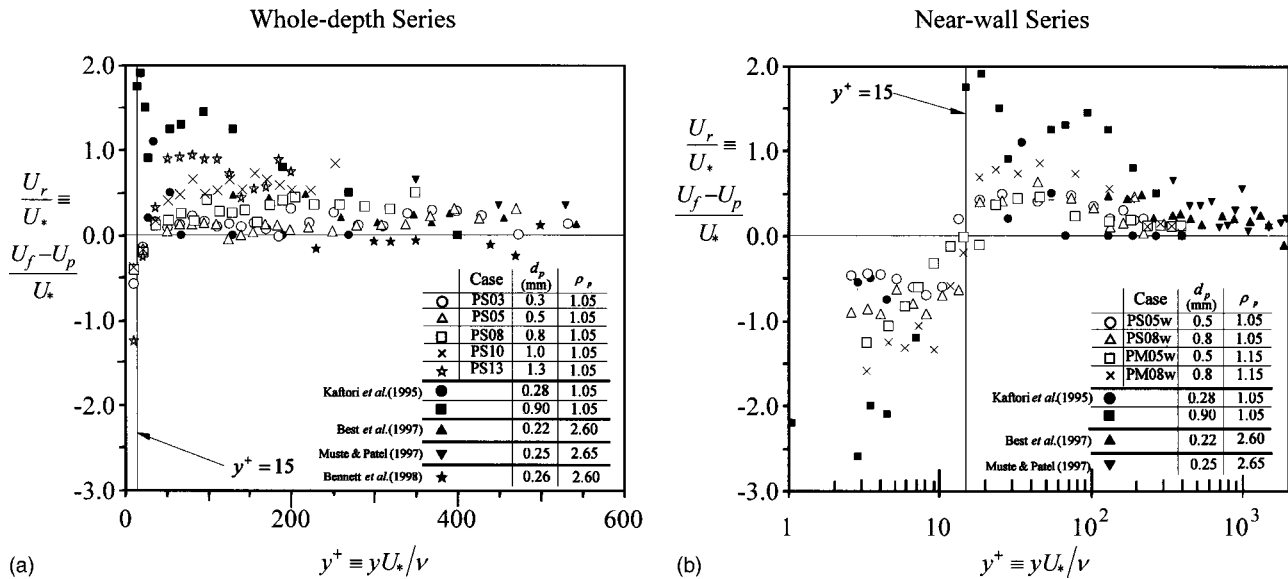


Fig. 10. Relative velocities between fluid and particles in two phase open-channel flows

gion. The most outstanding feature is that the average particle velocity  $U_p$  is smaller than the fluid velocity  $U_f$  in the region of  $y^+ \geq 15$ , whereas the former is larger than the latter in the viscous region of  $y^+ \leq 15$ . The features of the present data for  $\rho_p = 1.05$  and 1.15 agree with those of Kaftori et al.'s (1995) data for  $\rho_p = 1.05$ . The effect of particle size on the relative velocity is more significant than that of specific density, which can also be explained by Eq. (16). Best et al. (1997) and Muste and Patel (1997) could measure the velocity only in the outer region farther from the wall of  $y^+ > 150$  and 300, respectively; they used the glass and sand particles (Table 1). Nino and Garcia (1996) measured the velocity of glass particles for ejections and sweeps by flow visualization. Although the average particle velocity  $U_p$  was not analyzed, the streamwise velocity of particles averaged for ejections was smaller than the fluid velocity  $U_f$ . However, the relative velocity near the wall is not yet clarified by using glass beads.

It should be noticed that the average velocity of particles is larger than that of carrier fluid in the viscous region ( $y^+ \leq 15$ ). This noticeable fact is caused by particles moving toward the wall having an inertial force and high momentum when they inrush into the near-wall region. In contrast, the fluid velocity is depressed by viscous effect as described by Eq. (1). Consequently, the fluid velocity  $U_f$  becomes smaller than the average particle velocity  $U_p$ , and thus the particles will in turn transport some momentum to fluid in the near-wall region. This momentum transfer from particles to fluid increases with the particle size and induces the flatter distributions of fluid velocity  $U_f$  very near the wall, as observed in Fig. 7. That is the result of fluid-particle interactions, i.e., the two-way coupling. Furthermore, the particle-particle collisions, i.e., the four-way coupling may occur very near the wall due to much higher concentration. These significant differences of velocity between fluid and particles around below  $y^+ = 15$  are very important to investigate sediment transport phenomena and to develop numerical models in two phase-flow approach.

### Modulation of Turbulence Intensities

It is one of the most challenging topics in particle-laden flows to investigate whether the turbulence intensities of fluid are en-

hanced or depressed by the presence of particles due to fluid-particle interactions. The streamwise and vertical components of turbulence intensities of fluid,  $u_f'$  and  $v_f'$ , are defined as the RMS values of turbulence. These present data are shown in Fig. 11, together with previous data of Lyn (1992), Best et al. (1997), Muste and Patel (1997), and Bennett et al. (1998); all of them have used the particles of  $\rho_p \approx 2.6$  and  $d_p \approx 0.2$  mm (see Table 1). Kaftori et al. (1998) examined the turbulence modulation in the experiments of Kaftori et al. (1995) with  $\rho_p = 1.05$ , and their data are also included in Fig. 11 for comparison because of the same density as us. For clear-water open channel flow, Nezu (1977) (cited from Nezu and Nakagawa 1993) proposed the following empirical formula on the basis of hot-film data:

$$\frac{u_{cw}'}{U_*} = 2.3 \exp(-y/h) \quad (17)$$

$$\frac{u_{cw}'}{U_*} = 1.27 \exp(-y/h) \text{ for } y/h \geq 0.1$$

in which the subscript cw denotes the clear-water flow. The curves of Eq. (17) are also included in Fig. 11. The experimental data for clear-water flows are in good agreement with Eq. (17) except for data of Best et al. (1997); their data are slightly larger than Eq. (17) about both and . It should be noticed that the data for particle-laden flows agree well with Eq. (17) except for very near the wall, irrespective of the particle diameter  $d_p$  and its density  $\rho_p$ . To further highlight the turbulence modulation, Fig. 12 shows the turbulence intensities of fluid for particle-laden flows that are normalized by those for the corresponding clear-water flow, i.e.,  $u_f'/u_{cw}'$  and  $v_f'/v_{cw}'$ , in the near-wall region. Evidently, the turbulence modulation by the presence of particles is negligible in the outer region farther from the wall, irrespective of the particle diameter and specific density. The values of  $u_f'/u_{cw}'$  and  $v_f'/v_{cw}'$  in Best et al. (1997) seem to be slightly small because of the larger values of  $u_{cw}'$  and  $v_{cw}'$  as mentioned above. No modulation of turbulence in the outer region is explained by the fact that the particle response time  $t_p$  is much smaller than the eddy turnover time  $t_e$ , which did not significantly induce the relative velocity between fluid and particles in the outer region, as

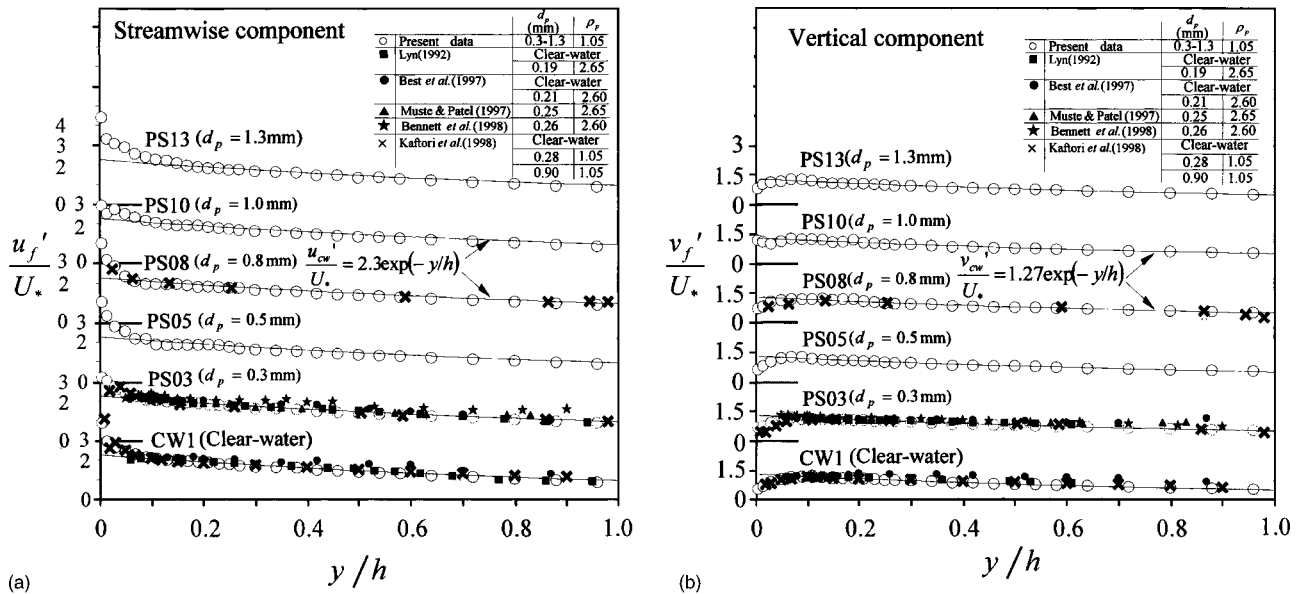


Fig. 11. Turbulence intensities of fluid,  $u_f'$  and  $v_f'$ , in two phase open-channel flows

discussed previously. Therefore, the particles can follow the carrier fluid motion substantially in the outer region and do not affect any turbulence modulation in fluid. Further, because the particle concentration is much smaller farther from the wall, the fluid-particle interaction seems to be negligibly small in the outer region. However, any significant suppression inferred from Fig. 6 may not occur in sediment-laden open channel flows, which will be different from gas-solid flows.

In contrast, it should be noticed that the turbulence intensities of fluid  $u_f'$  and  $v_f'$  are enhanced substantially by the presence of particles in the near-wall region of  $y^+ \leq 15$ , in which the particle velocity is larger than the fluid velocity as seen in Fig. 10. Of particular significance is that the vertical component  $v_f'$  of turbulence intensity is more enhanced by the particles than the streamwise component  $u_f'$ . Similar results were also obtained by Kafrori

et al. (1998) in Fig. 12. It is considered that the vertical component  $v_f'$  is apt to be more affected by the lift-up and settle-down motions of particles, i.e., the vertical motion. This suggests in turn the importance of interaction between the coherent bursting phenomena of fluid and the particle motion, as pointed out by Nino and Garcia (1996).

Simultaneous measurements of fluid and particles in a volume-averaged sense (see Crowe et al. 1996) were conducted successfully in this study, and the turbulence intensities of particles,  $u_p'$  and  $v_p'$ , were obtained in the same manner as those of fluid,  $u_f'$  and  $v_f'$ . The turbulence-intensity ratios of particles to fluid  $u_p'/u_f'$  and  $v_p'/v_f'$  are shown in Fig. 13, together with data of Muste and Patel (1997). The turbulence intensities of particles are nearly equal to those of carrier fluid farther from the wall, i.e.,  $u_p' \cong u_f'$  and  $v_p' \cong v_f'$ . The values of  $v_p'/v_f'$  in Muste and Patel (1997) are slightly smaller than the unity, and this might be caused by larger settling velocity due to higher specific gravity. Of particular significance is that the turbulence intensities of particles become larger than those of fluid in the near-wall region of  $y^+ \leq 15$ . This feature is much more remarkable in the vertical component  $v_p'$  than in the streamwise one  $u_p'$ . This suggests that the particle-particle collisions in addition to the fluid-particle interactions may not be neglected in the near-wall region of  $y^+ \leq 15$  and that the vertical movements of particles are more enhanced due to the ejections and sweeps, as inferred by Nino and Garcia (1996).

### Ejections and Sweeps for Fluid and Particles

The ejections and sweeps in bursting motion over smooth wall are analyzed by the quadrant theory of the instantaneous Reynolds stress of fluid  $-u_f(t)v_f(t)$  (see Nakagawa and Nezu 1977). The contributions of ejections RS2 and sweeps RS4 are defined as follows:

$$(RS2)_f = \begin{cases} -D(t) \cdot u_f(t)v_f(t) & \text{for } u_f < 0, v_f > 0 \\ 0 & \text{otherwise} \end{cases} \quad (18)$$

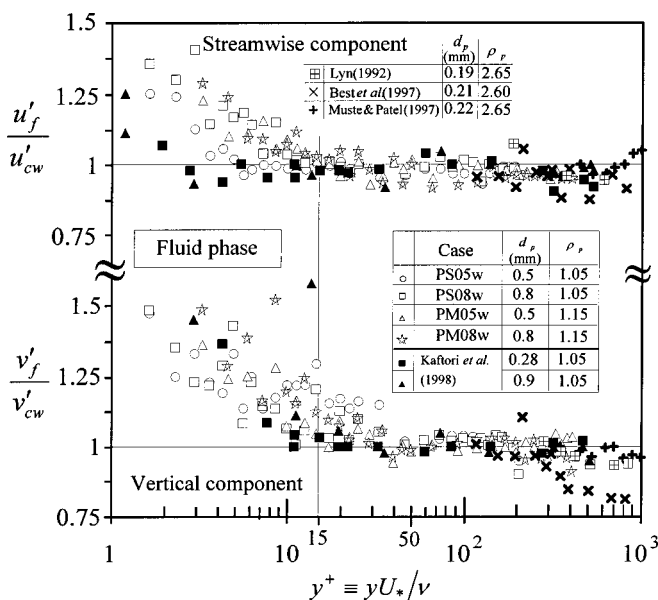


Fig. 12. Ratio of turbulence intensities to those for clear-water flow (turbulence modulation)

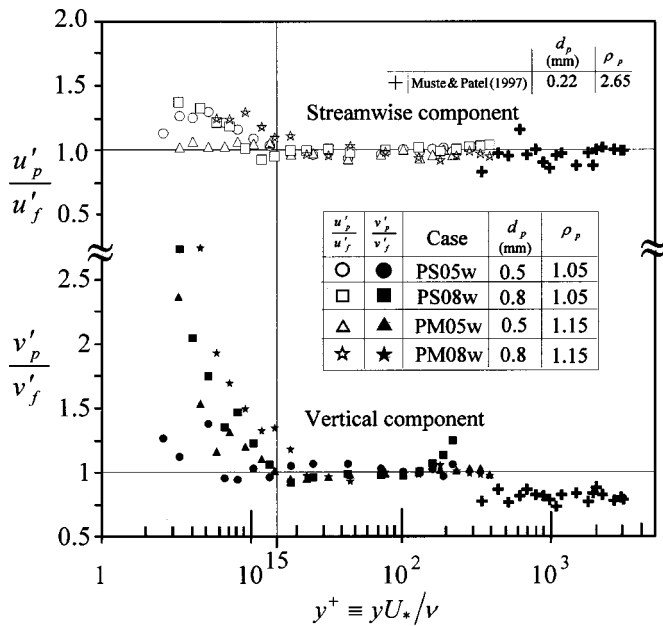


Fig. 13. Relation of turbulence intensities between particles and fluid

$$(RS4)_f = \begin{cases} -D(t) \cdot u_f(t)v_f(t) & \text{for } u_f > 0, v_f < 0 \\ 0 & \text{otherwise} \end{cases} \quad (19)$$

in which the discrimination function  $D(t)$  is given by

$$D(t) = \begin{cases} 1 & \text{if } |u_f(t)v_f(t)| \geq H u'_f v'_f \\ 0 & \text{otherwise} \end{cases} \quad (20)$$

The threshold value  $H$  is sometimes set as  $H=1$  in order to distinguish the bursting events from noncoherent ejection-like and sweep-like turbulence in clear-water flows although a definite value of  $H$  is not established even now. The value of  $H=0$  has been used in Wallace et al. (1972), Brodkey et al. (1974), and Nakagawa and Nezu (1977). However, it may be better to use the nonzero threshold value because the larger events would contribute more to the particle motion and also the hole data near  $H=0$  may be prone to include measurement errors. Similar suggestions are given in Bennett et al. (1998). So, this study has chosen  $H=1$ .

In the same manner, this quadrant theory is now applied to the particle motion in two phase flow. The contributions of ejections and sweeps for particle motion are defined as  $(RS2)_p$  and  $(RS4)_p$ , respectively, in which  $H=1$  was also chosen. Fig. 14 shows the results of  $(RS4)_f/(RS2)_f$  for fluid and  $(RS4)_p/(RS2)_p$  for particles. For comparison, Fig. 14 also shows the hot-film data of Wallace et al. (1972) and Brodkey et al. (1974) and the DNS data of Kim et al. (1987) in particle-free channel flows, which correspond to clear-water open channel flow. The present values of  $(RS4)_f/(RS2)_f$  in particle-laden flows are in good agreement with those in clear-water flows even in the near-wall region, where turbulence intensities are enhanced by the presence of particles, as seen in Fig. 12. The particles do not change the basic structure of bursting events drastically so that the sweeps of RS4 become larger than the ejections of RS2 in the near-wall region of  $y^+ \leq 15$ , while  $RS2 > RS4$  in the outer region of  $y^+ \geq 15$ . The present values of  $(RS4)_p/(RS2)_p$  for particles are similar to those for fluid. However, the sweeps of particles become more significant

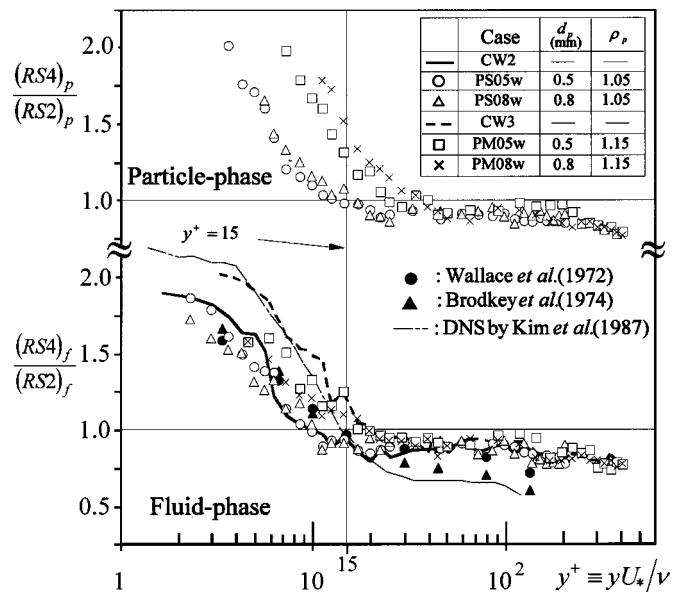


Fig. 14. Ratio of sweeps to ejections in the case of particle and fluid phases

in the near-wall region with an increase of the particle diameter  $d_p$  and its density  $\rho_p$ , although the present experimental conditions of  $d_p$  and  $\rho_p$  are limited in a narrow range.

Fig. 15 shows the variations of  $(RS2)_p/(RS2)_f$  and  $(RS4)_p/(RS4)_f$ . It seems that the ejections and sweeps of particles occur more violently than those of fluid, with an increase of  $d_p$  and  $\rho_p$ . The heavier-than-fluid particles are lifted up from the viscous sublayer by the ejections of fluid opposite to gravity, and hence the ejections of particles will be generated by only larger ejections of fluid, i.e.,  $(RS2)_p \geq (RS2)_f$  in the time-averaged sense. On the other hand, the suspended particles having high momentum will be encountered by eddies and inrushed into the near-wall region by sweeps of fluid, and otherwise some particles have settled down toward the wall by gravity. Therefore, the sweeps of particles become larger than those of fluid. This is due to the grain inertia effect. The particle-particle collisions will also contribute to larger ejections and sweeps of particles.

Nevertheless, the fluid sweeps are much more contributory to the motion of particles than the fluid ejections in the near-wall region of  $y^+ \leq 15$ . In turn, the particle sweeps seem to enhance the turbulence intensities of  $u'_f$  and  $v'_f$ , as seen in Fig. 12. Also, the particle sweeps will transport the high momentum to fluid, and consequently the velocity gradient of fluid will become flatter in the viscous sublayer as seen in Fig. 7. These phenomena are caused by the fluid-particle interactions, and also probably by the particle-particle interactions because of high concentration very near the wall. Therefore, it is further necessary to investigate such interactions between bursting events and particle motion due to two-way and four-way couplings in a wide range of particle diameter, specific density, and concentration.

## Conclusions

In this study, simultaneous measurements of both the particles and fluid (water) were conducted in particle-laden open channel flows by means of a discriminator PTV. The mean velocity and turbulence characteristics for fluid and particles each were exam-

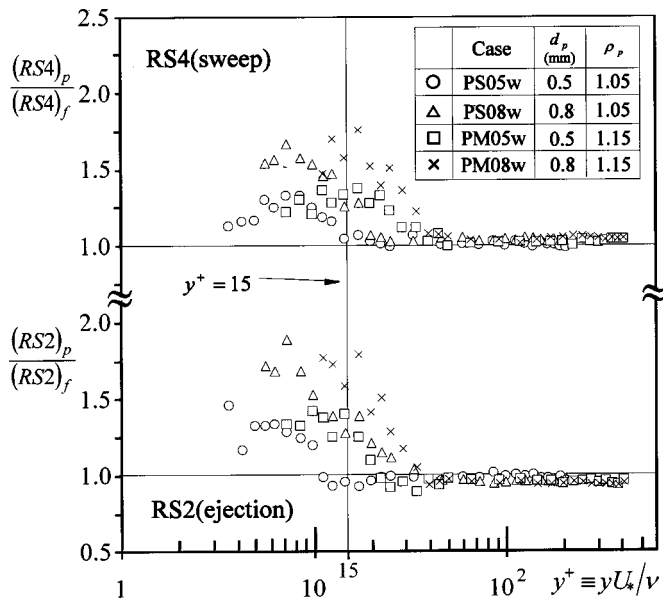


Fig. 15. Relations of ejections and sweeps between particles and fluid

ined in comparison with those in clear-water (particle-free) flow, together with previous existing LDA and PDA data. The main findings obtained in this study are as follows:

1. The measured values of Reynolds stress for fluid were in good agreement with the theoretical formula in the outer region. Consequently, the friction velocity could be reasonably evaluated from the measured Reynolds stress even in two phase flows. The normalized fluid-velocity profiles in two phase flows are described well by the log-law in the inner-wall region. However, the value of the von Karman constant decreases slightly with an increase of the particle concentration.
2. The average particle velocity is slightly smaller than the carrier-fluid velocity farther from the wall. In contrast, of particular significance is that the average particle velocity is larger than the fluid velocity very near the wall. The relative velocity difference between particles and fluid causes the fluid-particle interactions, in which the relation between the particle response time and the eddy turnover time plays an important role.
3. The turbulence intensities are not almost modulated by the presence of particles farther from the wall, irrespective of the particle diameter and specific density. In contrast, the turbulence intensities of fluid are enhanced substantially by the presence of particles in the near-wall region.
4. The turbulence intensities of particles become further larger than those of fluid in the near-wall region. The vertical component of particles is more marked than the streamwise one, which infers that the vertical movements of particles are more enhanced due to the ejections and sweeps.
5. The fluid sweeps are more contributory to the motion of particles than the fluid ejections in the near-wall region. In turn, the particle sweeps seem to enhance the turbulence intensities of fluid. Also, the particle sweeps will transport the high momentum to carrier fluid, and consequently the velocity gradient of fluid becomes flatter in the viscous sublayer. These phenomena are caused by the fluid-particle interactions, and also probably by the particle-particle interactions

because of high concentration very near the wall.

Therefore, it is further necessary to investigate such interactions between bursting events and particle motion due to two-way and four-way couplings in a wide range of particle diameter, specific density, and sediment concentration, and then to develop reasonable computer simulation models of two phase open channel flow.

## References

- Bennett, S.J., Bridge, J. S., and Best, J. L. (1998). "Fluid and sediment dynamics of upper stage plane beds." *J. Geophys. Res., [Oceans]*, 103, 1239–1274.
- Best, J., Bennett, S., Bridge, J., and Leeder, M. (1997). "Turbulence modulation and particle velocities over flat sand beds at low transport rate." *J. Hydraul. Eng.*, 123(12), 1118–1129.
- Brodkey, R. S., Wallece, J. M., and Eckelmann, H. (1974). "Some properties of truncated turbulence signals in bounded shear flow." *J. Fluid Mech.*, 63, 209–224.
- Cioffi, F., and Gallerano, F. (1991). "Velocity and concentration profiles of solid particles in a channel with movable and erodible bed." *J. Hydraul. Res.*, 29, 387–401.
- Crowe, C. T., Troutt, T. R., and Chung, J. N. (1996). "Numerical models for two phase turbulent flows." *Annu. Rev. Fluid Mech.*, 28, 11–43.
- Elghobashi, S. (1994). "On predicting particle-laden turbulent flows." *Appl. Sci. Res.*, 52, 309–329.
- Elghobashi, S., and Truesdell, G. C. (1993). "On the two-way interaction between homogeneous turbulence and dispersed solid particles. 1. Turbulence modification." *Phys. Fluids A*, 5, 1790–1801.
- Gore, R. A., and Crowe, C. T. (1989). "Effect of particle size on modulating turbulent intensity." *Int. J. Multiphase Flow*, 15, 279–285.
- Guo, J., and Julien, P. Y. (2001). "Turbulent velocity profiles in sediment-laden flows." *J. Hydraul. Res.*, 39, 11–23.
- Kaftori, G., Hetsroni, G., and Banerjee, S. (1995). "Particle behavior in the turbulent boundary layer. II. Velocity and distribution profiles." *Phys. Fluids*, 7, 1107–1127.
- Kaftori, G., Hetsroni, G., and Banerjee, S. (1998). "The effect of particles on wall turbulence." *Int. J. Multiphase Flow*, 24, 359–386.
- Kim, J., Moin, P., and Moser, R. (1987). "Turbulence statistics in fully developed channel flow at low Reynolds number." *J. Fluid Mech.*, 177, 133–166.
- Kulick, J. D., Fessler, J. R., and Eaton, J. K. (1994). "Particle response and turbulence modification in fully developed channel flow." *J. Fluid Mech.*, 277, 109–134.
- Lyn, D. A. (1991). "Resistance in flat-bed sediment-laden flows." *J. Hydraul. Eng.*, 117(1), 94–114.
- Lyn, D. A. (1992). "Turbulence characteristics of sediment-laden flows in open channels." *J. Hydraul. Eng.*, 118(7), 971–988.
- Muste, M. (2002). "Sources of bias errors in flume experiments on suspended-sediment transport." *J. Hydraul. Res.*, 40, 695–708.
- Muste, M., and Patel, V. C. (1997). "Velocity profiles for particles and liquid in open-channel flow with suspended sediment." *J. Hydraul. Eng.*, 123(9), 742–751.
- Nakagawa, H., and Nezu, I. (1977). "Prediction of the contributions to Reynolds stress from bursting events in open-channel flows." *J. Fluid Mech.*, 80, 99–128.
- Nezu, I. (1977). "Turbulence intensities in open-channel flows." *Proc., JSCE*, 261, 67–76 (in Japanese).
- Nezu, I., Esaki, K., and Onitsuka, K. (1999). "Interaction between turbulent structure and bed-load transport in open-channel flows." *Hydraulic modeling*, V. P. Singh et al., eds., Water Resources, Lakewood, Colo., 63–76.
- Nezu, I., and Nakagawa, H. (1993). *Turbulence in open channel flows*. IAHR Monograph, Balkema, Rotterdam, The Netherlands.
- Nezu, I., and Onitsuka, K. (2001). "Turbulent structures in partly vegetated open-channel flows with LDA and PIV measurement." *J. Hy-*

- draul. Res.*, 39, 629–642.
- Nezu, I., Onitsuka, K., and Azuma, R. (2001). “Turbulence measurements of open-channel flows over gravel bed.” *Proc., 3rd Int. Symp. on Measurement Techniques for Multiphase Flows*, Fukui, Japan, 266–272.
- Nezu, I., and Rodi, W. (1986). “Open-channel flow measurements with a laser Doppler anemometer.” *J. Hydraul. Eng.*, 112(5), 335–355.
- Nino, Y., and Garcia, M. H. (1996). “Experiments on particle-turbulence interactions in the near-wall region of an open channel flow: implications for sediment transport.” *J. Fluid Mech.*, 326, 285–319.
- Okamoto, K., Hassan, Y. A., and Schmidl, W. D. (1995). “New tracking algorithm for particle image velocimetry.” *Exp. Fluids*, 19, 342–347.
- Pedinotti, S., Mariotti, G., and Banerjee, S. (1992). “Direct numerical simulation of particle behaviours in the wall region of turbulent flows in horizontal channels.” *Int. J. Multiphase Flow*, 18, 927–941.
- Rashidi, M., Hetsroni, G., and Banerjee, S. (1990). “Particle-turbulence interaction in a boundary layer.” *Int. J. Multiphase Flow*, 16, 935–949.
- Rogers, C. B., and Eaton, J. K. (1990). “The behavior of solid particles in a vertical turbulent boundary layer in air.” *Int. J. Multiphase Flow*, 16, 819–834.
- Rogers, C. B., and Eaton, J. K. (1991). “The effect of small particles on fluid turbulence in a flat-plate, turbulent boundary layer in air.” *Phys. Fluids A*, 3, 928–937.
- Squires, K. D., and Eaton, J. K. (1990). “Particle response and turbulence modification in isotropic turbulence.” *Phys. Fluids A*, 2, 1191–1203.
- Sumer, B. M., and Deigaard, R. (1981). “Particle motions near the bottom in turbulent flow in an open channel. Part 2.” *J. Fluid Mech.*, 109, 311–337.
- Wallace, J. M., Eckelmann, H., and Brodkey, R. S. (1972). “The wall region in turbulent shear flow.” *J. Fluid Mech.*, 54, 39–48.
- Yalin, M. (1972). *Mechanics of sediment transport*, Pergamon, New York.